The alternative complement pathway regulates pathological angiogenesis in the retina

J. Harry Sweigard,* Ryoji Yanai,* Philipp Gaissert,* Magali Saint-Geniez,† Keiko Kataoka,* Aristomenis Thanos,* Gregory L. Stahl,‡ John D. Lambris,§ and Kip M. Connor*,[1]

*Angiogenesis Laboratory, Department of Ophthalmology, and †Schepens Eye Research Institute, Massachusetts Eye and Ear Infirmary, and ‡Center for Experimental Therapeutics and Reperfusion Injury, Department of Anesthesiology, Perioperative, and Pain Medicine, Brigham and Women's Hospital, Harvard Medical School, Boston, Massachusetts, USA; and §Department of Pathology and Laboratory Medicine, University of Pennsylvania, Philadelphia, Pennsylvania, USA

ABSTRACT **A defining feature in proliferative retinopathies is the formation of pathological neovessels. In these diseases, the balance between neovessel formation and regression determines blindness, making the modulation of neovessel growth highly desirable. The role of the immune system in these retinopathies is of increasing interest, but it is not completely understood. We investigated the role of the alternative complement pathway during the formation and resolution of aberrant neovascularization. We used alternative complement pathway–deficient ($Fb^{-/-}$) mice and age- and strain-matched control mice to assess neovessel development and regression in an oxygen-induced retinopathy (OIR) mouse model. In the control mice, we found increased transcription of *Fb* after OIR treatment. In the $Fb^{-/-}$ mice, we prepared retinal flatmounts and identified an increased number of neovessels, peaking at postnatal day 17 (P17; $P=0.001$). Subjecting human umbilical vein endothelial cells (HUVECs) to low oxygen, mimicking a characteristic of neovessels, decreased the expression of the complement inhibitor *Cd55*. Finally, using laser capture microdissection (LCM) to isolate the neovessels after OIR, we found decreased expression of *Cd55* ($P=0.005$). Together, our data implicate the alternative complement pathway in facilitating neovessel clearance by down-regulating the complement inhibitor Cd55 specifically on neovessels, allowing for their targeted removal while leaving the established vasculature intact.—Sweigard, J. H., Yanai, R., Gaissert, P., Saint-Geniez, M., Kataoka, K., Thanos, A., Stahl, G. L., Lambris, J. D., Connor, K. M. The alternative complement pathway regulates pathological angiogenesis in the retina. *FASEB J.* 28, 3171–3182 (2014). www.fasebj.org**

Key Words: neovascularization · innate immune system · factor b · Cd55 · oxygen-induced retinopathy

Angiogenesis is a tightly regulated process by which endothelial cells proliferate and migrate to colonize tissues, resulting in the establishment of an ornate network of vasculature that supports the vital systems of the body (1). However, when misdirected, pathological angiogenesis manifests in disease processes, such as cancer (1), atherosclerosis (2), and ocular neovascularization [ref. 3; diabetic retinopathy (DR), ref. 4, and retinopathy of prematurity (ROP), ref. 5]. DR and ROP both have in common late-stage destructive neovascularization (6) that is associated with inflammation (7, 8). Retinopathy begins with an initial phase of vessel loss (3), which then leads to local tissue hypoxia and a compensatory angiogenic response that is often pathological (6, 9). In ROP, pathological neovascularization regresses in most cases, leaving normal vessels intact, but persistent neovessels can cause progression to blindness, if unchecked (10). Inflammation is closely linked to vascular injury and repair (7, 11), which is mediated, in part, by the complement system and is likely to be a critical component of retinopathy (12). We hypothesized that neovessels can be distinguished from normal vessels and pruned through activation of the complement cascade.

The complement system is capable of distinguishing among healthy and diseased host cells, to aid in the elimination of nonfunctional or dead self-cells (13). The complement system consists of 3 pathways (classical, lectin, and alternative) that aid in the opsonization

Abbreviations: DR, diabetic retinopathy; EdU, 5-ethynyl-2′-deoxyuridine; Fb, factor b; HUVEC, human umbilical vein endothelial cell; INL, inner nuclear layer; LCM, laser capture microdissection; MAC, membrane attack complex; OIR, oxygen-induced retinopathy; ONL, outer nuclear layer; P, postnatal day; ROP, retinopathy of prematurity; RPE, retinal pigment epithelium; TUNEL, terminal deoxynucleotidyl dUTP nick end labeling; Vegf, vascular endothelial growth factor; VegfR, Vegf receptor

[1] Correspondence: Massachusetts Eye and Ear Infirmary, Harvard Medical School, 243 Charles Street, Boston, MA 02114, USA. E-mail: kip_connor@meei.harvard.edu

doi: 10.1096/fj.14-251041

This article includes supplemental data. Please visit *http://www.fasebj.org* to obtain this information.

and removal of irreversibly damaged tissue and/or pathogens (14). The classical pathway is activated by C1q's recognition of antigen–antibody interactions and the lectin pathway through pattern recognition of carbohydrate motifs by its mannose-binding lectin (14). Contrary to the classical and lectin pathways, the alternative pathway is not activated through recognition of pattern motifs; it probes its surroundings by maintaining a slow, steady state of activation through the hydrolysis of the pathway's central C3 molecule, to form $C3_{H2O}$ (15). When a small fraction of C3 is converted into $C3_{H2O}$, new sites are exposed that enable binding of factor b (Fb), leading to a short-lived, solvent-based C3 convertase that cleaves C3 into its active component, C3b (13). Newly generated C3b attaches to the surface of pathogens or dying cells through covalent binding, where it recruits Fb. Factor d (Fd) then cleaves Fb into Bb and forms the C3 convertase, C3bBb (16). Formation of the C3 convertase is a pivotal turning point for the amplification of the alternative pathway with Fb as a rate-limiting protein in its formation (16). It triggers a switch from slow hydrolysis of the central C3 protein to active cleavage by the convertase, which rapidly amplifies the alternative pathway and facilitates elimination of damaged or dead cells (13). Nondamaged self-cells express inhibitors of the complement system on their surface that prevent complement activation on healthy tissue, including Cd46 (17), Cd55 (18), and Cd59 (19, 20). These molecules degrade or sequester complement proteins and prevent their activation (13, 21).

In this study, we investigated whether the invoked inflammatory response inherent in retinopathy is involved in resolution of retinal neovascularization, distinguishing pathological neovessels from normal vessels. We characterized the role of the alternative complement pathway in the formation and clearance of pathological neovessels in a mouse model of oxygen-induced retinopathy (OIR; ref. 3). Understanding how the ocular environment can target pathological vessels for elimination while leaving the essential vasculature intact will lend insight into ways of safely modulating the microenvironment without causing harm and lead to the development of pharmaceuticals that take advantage of the same targeting strategy.

MATERIALS AND METHODS

Animals and model of OIR

This study adhered to the Association for Research in Vision and Ophthalmology (ARVO) Statement for the Use of Animals in Ophthalmic and Vision Research. C57Bl/6 mice (stock no. 000664) were obtained from Jackson Laboratories (Bar Harbor ME, USA), and $Fb^{-/-}$ mice were a gift from J.D.L. Each strain was maintained as a breeding colony in the Massachusetts Eye and Ear Infirmary (MEEI) animal facility. A published model of OIR causing ROP was used (9). Briefly, newborn mice and nursing mothers were kept in room air from postnatal day 0 (P0) to P7. At P7, each nursing mother and litter (≤8 pups) were placed in a chamber maintained at 75% oxygen (model 110; Biospherix, Lacona, NY, USA) for 5 consecutive days. At P12, the nursing mothers and litters were returned to room air, and samples were collected at the indicated time points. Pups from each litter were spread over the collection time course and weighed at P17. Litters with pups < 5 g at P17 were not included for analysis, since this weight has been deemed the minimum that ensures proper nursing and the transfer of growth factors for neovessel formation (9). The eyes were enucleated with the mice under heavy anesthesia (T4, 840-2; Avertin; 2,2,2 tribromoethanol; Sigma-Aldrich, St. Louis, MO, USA, in isoamyl alcohol, A730-1; Thermo Scientific, Waltham, MA, USA), at a working concentration of 10 mg/ml, injected at a dose of 0.25–0.5 mg/g intraperitoneally.

Retinal flatmounts

After OIR treatment, the eyes were enucleated from P14 through P17, P21, and P25; fixed in 4% PFA for 1 h at 25°C; transferred to PBS; and stored at 4°C. The retinas were separated by dissection, with care taken to remove the remaining hyaloid vasculature, and permeabilized overnight at 4°C with 1% Triton X-100 (T-8787; Sigma-Aldrich) in PBS. The following day, the samples were incubated in isolectin B4 conjugated to 568 (GS-IB4; I21412; Life Technologies, Carlsbad, CA, USA) at a dilution of 1:50 in 1 mM $CaCl_2$ solution at 25°C overnight in the dark on a rotating platform. After 3 washes in 1× PBS over the course of 2 h, the retinas were cut into a cross shape and coverslipped with antifade reagent in glycerol/PBS (S2828; Invitrogen). Images of the flatmounts were captured at ×5 using an AxioVision microscope and stitched together with AxioVision 4.8.2 software (Zeiss, Thornwood, NY, USA). For quantification, the stitched images were saved as TIFF files, and the percentage of neovascular area was calculated with PhotoShop, version CS5 (Adobe Systems, San Jose, CA, USA; ref. 9). Briefly, using the Magic Wand tool in CS5, we chose a threshold that selectively captured the pixel intensity of the neovessels. Further refinement to isolate only neovessels was manually performed by using the Magic Wand tool to add neovessels that had been missed, by tapping the center of the missed neovessels or by deleting areas that were not neovessels by pressing Control+Alt+Z. The amount of neovessels was determined by dividing the number of pixels of neovessels by the number of pixels of total retinal area and multiplying by 100.

Immunohistochemistry

At the indicated time points after OIR treatment, the eyes were enucleated and quickly frozen in optimal cutting temperature (OCT) compound (4583; Tissue Tek; Sakura Finetek, Torrance, CA, USA) by submersion in a beaker of isopropanol chilled by dry ice. Cryosections were cut at 14 μm and fixed for 20 min in 4% PFA. Before incubation in primary antibody, the sections were blocked for 1 h in PBS containing 5% fetal calf serum, 0.3% Triton X-100, and 0.5% bovine serum albumin. For Fb and isolectin B4 colabeling, an antibody to Fb (SC67141; Santa Cruz Biotechnology, Dallas, TX, USA) was used at a dilution of 1:50 in 1 mM $CaCl_2$ containing a 1:50 dilution of isolectin B4–Alexa Fluor 488 conjugate (I21411; Life Technologies). The samples were incubated overnight in a humidified chamber at 4°C. All secondary detection was performed with either donkey anti-rabbit conjugated to Alexa Fluor 647 (A31573; Life Technologies) or goat anti-rabbit conjugated to Alexa Fluor 568 (A11008; Life Technologies) at a dilution of 1:750 in PBS and incubated at room temperature in the dark with gentle

rotation for 1 h. After a wash in PBS, the sections were coverslipped with Vectashield containing DAPI (H-1200; Vector Laboratories, Burlingame, CA, USA). For terminal deoxynucleotidyl dUTP nick end labeling (TUNEL) and isolectin B4 colabeling, the sections were incubated in isolectin B4 conjugated to Alexa Fluor 488 (I21411; Life Technologies) at a concentration of 1:50 in 1 mM $CaCl_2$ overnight at 25°C, in the dark with gentle agitation. After several washes, TUNEL labeling (12156792910; Roche, Indianapolis, IN, USA) was performed according to the kit instructions, and the sections were mounted in Vectashield.

Western blot analysis

The retinas were lysed in M-PER lysis buffer (78501; Thermo Scientific) containing Halt phosphatase inhibitor cocktail (1862495; Thermo Scientific) and Complete protease inhibitor cocktail (1862209; Thermo Scientific). Equal volumes of protein were added to a NuPage 4–12% Bis-Tris gel (NP0335BOX; Life Technologies), transferred, and probed for mouse vascular endothelial growth factor receptor 2 (VegfR2) with a rabbit monoclonal antibody (2479; Cell Signaling Technology, Danvers, MA, USA) at 1:1000 for 3 h at room temperature in a sealed bag. Secondary detection was achieved using ECL Select (RPN2235; GE Healthcare, Cleveland, OH, USA) at a concentration of 1:20,000. Bands were normalized with β-actin (4970; Cell Signaling Technology). Quantification of band intensities was performed with a Chemidoc MP Station and Image Lab 4.1 software (Bio-Rad, Hercules, CA, USA).

Quantitation of proliferation in neovessels

After the OIR treatment, the mice were injected with 5-ethynyl-2′-deoxyuridine (EdU; C10337; Life Technologies) at P13 and P15 at a dose of 50 mg/kg in a final volume of 40 μl. The eyes were enucleated at P17, frozen, and sectioned as for immunohistochemistry. The weight of the mice at P17 was ≥5 g, to ensure sufficient nursing from the mother for growth factor nourishment (9). Four regions of each eye were taken at 100 μm intervals through the eye, to ensure representative quantification of each eye. Quantification of proliferating cells in the neovessels was performed by counting the total number of EdU-positive cells in an isolectin-labeled neovessel, dividing by the neovascular area, and multiplying by 100 to arrive at the percentage of cells proliferating in the neovessel.

Quantitation of apoptosis in neovessels

After OIR treatment, the eyes were enucleated at P17, frozen, and sectioned for immunohistochemistry. The weight of the mice and sectioning of the eyes was the same as for quantification of neovessel proliferation. Quantification of apoptotic cells in neovessels was performed by counting the total number of TUNEL-positive cells in an isolectin-labeled neovessel, dividing by the total number of DAPI-positive cells in the same isolectin-labeled neovessel, and multiplying by 100 to arrive at the percentage of apoptotic cells in the neovessel.

Laser capture microdissection (LCM)

Eyes were enucleated at P17, placed in OCT compound, and quickly frozen by submersion in a beaker of isopropanol chilled by dry ice. Between 16 and 18 sections cut at 30 μm thickness were placed on a frame slide (11505190; Leica Microsystems, Wetzlar, Germany) and allowed to air dry for 10 min. All reagents were made with nuclease-free water (AM9932; Ambion, Carlsbad, CA, USA). The sections on the frame slides were fixed with a graded series of ethanol (459836-1L; Sigma-Aldrich), consisting of incubation in 50% ethanol for 1 min, 75% ethanol for 1.5 min, and water for 1 min. To label the vessels and neovessels, the sections were incubated in isolectin B4 conjugated to HRP (L5391; Sigma-Aldrich) diluted 1:50 in 1 mM $CaCl_2$ for 15 min at 25°C. After the slides were washed in PBS, color was generated by adding DAB (K3467; DakoCytomation-Agilent, Carpinteria, CA, USA) for 2 min. To identify the cell layers, the slides were dipped in 0.1% toluidine blue solution (89640-5G; Fluka, St. Louis, MO, USA) followed by 2 rinses in water for 15 s each, in 75% ethanol for 30 s, and in water for 15 s. Sections were dried in room air, and the inner nuclear layer (INL), outer nuclear layer (ONL), and retinal pigment epithelium (RPE) and vessels and neovessels were isolated by LCM (LMD 7000; Leica Microsystems). Samples were collected in RNAlater (AM7022; Ambion) and stored at −80°C until RT-PCR was performed.

RT-PCR

RNA was isolated by using an RNeasy micro kit (74004; Qiagen, Valencia, CA, USA) for LCM samples or an RNeasy mini kit (74106; Qiagen) for whole retina. RNA was measured with a Nanodrop spectrophotometer (model 2000; Thermo Scientific) and normalized to the same amount of RNA before the cDNA was transcribed with Superscript III (18080-044; Invitrogen). A volume of 1 μl of cDNA was used for each RT-PCR reaction in KAPA SYBR Fast universal master mix (KK4600; KAPA Biosystems, Wilmington, MA, USA) on a Step One Plus real-time PCR system (Applied Biosystems). Primers for Fb and Cd55 (mouse) were obtained from Integrated DNA Technologies (Coralville, IA, USA), by using their online Primer Quest design tool and importing the U.S. National Center for Biotechnology Information (NCBI; Bethesda, MD, USA) ID number for each sequence. The primer for Cd55 (human) was *Taq*man (Hs00892618_m1; Life Technologies). RT-PCR was run in triplicate, and the average of each C_T value was used for analysis. All C_T values were normalized to β-actin from each sample as an internal control. Final values were determined by the $\Delta\Delta C_T$ method.

RT-PCR for Vegf isoforms

mRNA (500 ng) was transcribed with the Iscript kit (Bio-Rad). Real-time PCR was performed with FastStart SYBR Green master mix on the LightCycler 480 real-time PCR system (Roche Applied Science). Vegf isoform expression was determined by using the absolute quantification method after normalization with the housekeeping genes *cyclophilin-A* and β-*actin*. A standard curve was constructed for each PCR reaction and was derived from the serial dilution (3×10^1 to 3×10^6 copies/reaction) of a plasmid coding for each isoform, Vegf188, Vegf164, and Vegf120 (Supplemental Table S1 and ref. 22), and amplified by the SYBR Green system. The level of isoform expression in each sample was calculated relative to the standard curve. Results were recorded as means ± SEM.

ELISA

Whole retinas were isolated, flash frozen in liquid nitrogen, and stored at −80°C. Protein extraction from the retinas was performed with M-Per protein extraction reagent (78501; Thermo Scientific), and concentration was determined with the Bradford assay. ELISAs for Fb (BG-MUS10520; Novatein-

Bio, Woburn, MA, USA), according to the kit's instructions, and was measured with a Spectramax M3 plate reader (Molecular Devices, Sunnyvale, CA, USA). Standard curves were generated with the reagents provided in the kit, and the sample values were determined automatically with Softmax Pro software (Molecular Devices). Six retinas from each group per time point were used and plated in duplicate wells. ELISAs were all plated in duplicate wells and averaged for the final value.

Human umbilical vein endothelial cell (HUVEC) time course

In all experiments with HUVECs (PCS-100-010; ATCC, Manassas, VA, USA), the cells had been cultured for 8–15 passages. Six P60 plates were grown to 90% confluence in 20% O_2 and placed in 1% O_2 for 24 h in a tri-gas incubator that electronically regulates oxygen levels (Heracell 150i; Thermo Scientific). One plate was collected at 30 min, one at 1 h, and one at 24 h by scraping and then centrifuged at 1200 rpm for 3 min. The pellet was resuspended in 350 μl buffer RLT containing β-mercaptoethanol. The remaining 3 plates were moved from 1% O_2 back into 20% O_2 for another 24 h period. One plate was collected at 30 min, one at 1 h, and one at 24 h by the same procedure. Each 48 h time course was performed 3 times for triplicate experiments. RT-PCR was performed as described above.

Statistical analysis

Data were analyzed with an unpaired Student's *t* test. Results are expressed as means ± SEM (unless otherwise specified). Significance was set at $P < 0.05$.

RESULTS

Alternative pathway–deficient mice manifest increased neovessel development

The alternative complement pathway is remarkably fast at responding to local tissue changes by constantly probing the surroundings for pathogens or diseased tissue (14). Since neovessels are dysregulated in many respects, lacking several functional aspects of endothelium, we examined whether these pathological vessels could be a target of the alternative pathway.

To study the role of the alternative pathway in pathological neovascularization, we used a well-defined mouse model of OIR (ref. 3 and **Fig. 1**), in combination with mice deficient in the alternative complement pathway ($Fb^{-/-}$). The OIR model consists of 2 distinct phases. In the first phase, P7 through P12, mice are placed in a high-oxygen environment that results in vasoobliteration of the developing vasculature (3). The second phase begins when the mice are returned to atmospheric oxygen at P12. The relatively low oxygen concentration causes the central avascular zone to become hypoxic, inducing the expression of Hif-2α-mediated proangiogenic pathways and of VEGF (23, 24). Although these pathways stimulate the growth of normal vessels, they also cause the formation of pathological vessels (neovessels), which sprout from the superficial retinal vasculature (3). The growth of neovessels begins at P14, with the peak number at P17 (3). The abnormal neovessels are leaky, resembling the pathological neovascularization seen in humans with ROP and proliferative diabetic retinopathy (3). Given the complement system's role in the clearance of damaged or diseased tissue, we investigated whether the alternative complement pathway targets neovessels. Neovessel formation was assessed in $Fb^{-/-}$ mice deficient in Fb, a key mediator of the alternative pathway, during neovessel formation from P14 to P17. We found significantly more neovessels in the $Fb^{-/-}$ mice from P15 through P17 (**Fig. 2*A***). The most striking difference was observed at P17 (7.26±0.31 and 12.52±0.32% for WT and $Fb^{-/-}$, respectively), the height of neovessel formation (Fig. 2*A*, *B* and Supplemental Fig. S1). After P17, neovessels begin to resolve in the OIR model, similar to the spontaneous regression often seen in humans with ROP (3, 25). By P25, the retinal vasculature returns to a state of homeostasis where the neovessels disappear, and the retinal vascular plexus stabilizes (3). During this neovessel resolution phase, we found that the neovessels persisted for a longer period in the $Fb^{-/-}$ mice, with more neovessels remaining at P21 and P25 (Fig. 2*A* and Supplemental Fig. S1). Although regression took longer, the $Fb^{-/-}$ mice eventually returned to homeostasis, indicating that the alternative pathway plays a key role, but is not the sole pathway involved.

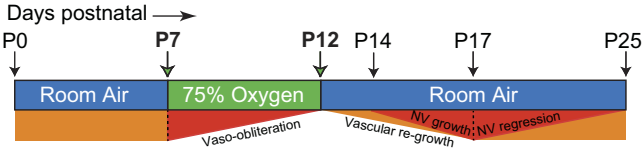

Figure 1. Mouse model of OIR. Time line depicting the age and amount of time either in room air or 75% O_2, to induce angiogenesis. The corresponding vascular changes that take place through the course of disease are labeled below the time course. Orange bars refer to normal vascular changes; red bars refer to diseased neovascular changes. NV, neovessel.

Proliferation of neovessels is unaltered in $Fb^{-/-}$ mice

The result of increased neovessels in the $Fb^{-/-}$ mice could be due to more rapid neovessel formation or from a deficiency in the removal of neovessels. In the OIR model, Vegf is known to play a critical role in neovessel formation (26). Therefore, a reasonable explanation for there being more neovessels in the $Fb^{-/-}$ mice would be increased Vegf expression. We first tracked the gene expression of Vegf164, the most prominent isoform of Vegf in the retina (27–30), in control mice exposed to OIR and, as expected, found that Vegf164 was suppressed when the mice were in high oxygen (P8H–12H), but rapidly increased on return to room air (P14–P17) (**Fig. 3*A*** and ref. 31). To determine whether Vegf could be responsible for more neovessel formation in the $Fb^{-/-}$ mice, we compared the relative expression levels of the *Vegf* isoforms *120*, *164*, and *188* at P17 and found no difference in

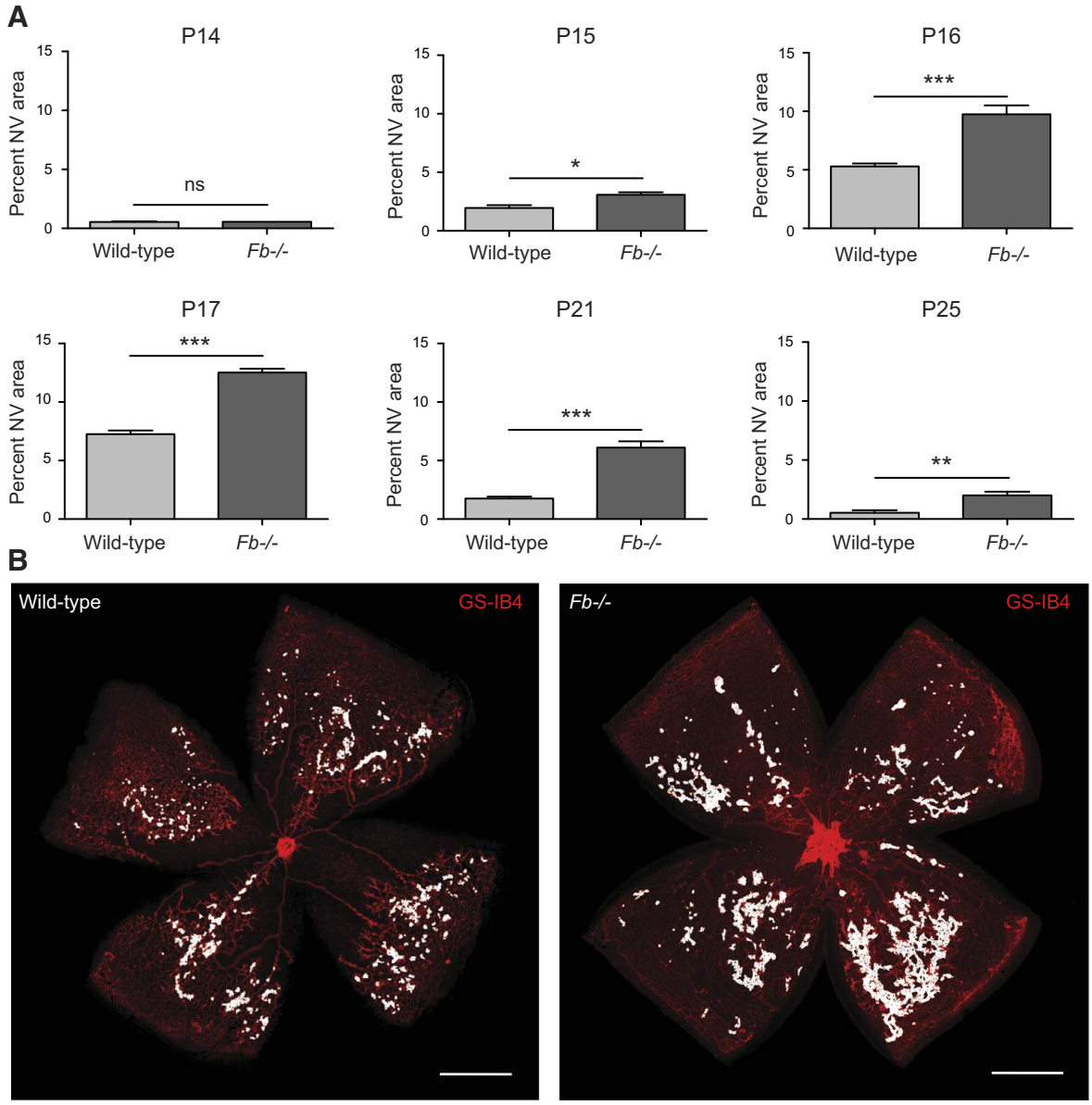

Figure 2. Loss of the alternative complement signaling cascade increases the severity and duration of retinopathy. *A*) Quantitation of neovessels (neovascular area) in $Fb^{-/-}$ mice compared to wild-type control mice after OIR (P14–P17, P21, and P25) measured as the total area of neovessels relative to the total retinal area in the flatmount after vascular labeling by isolectin B4. $Fb^{-/-}$ mice had a significant increase in neovessel development from P15 to P17 that persisted from P17 to P25, compared with that in the control animals. P14–P16, P21, and P25, n=18–20 eyes; P17, n=45 eyes. ns, not significant. Error bars = SEM. $^{*}P < 0.05$, $^{**}P < 0.01$, $^{***}P \leq 0.001$. *B*) Representative flatmount images at P17 after OIR; vessels were labeled with isolectin B4 (red). White areas are neovessels that were selected for quantitation by Photoshop. Scale bars = 1 mm.

expression levels among any of the isoforms between the control and $Fb^{-/-}$ mice (Fig. 3*B*). Since increases in Vegf signaling could also be a consequence of more VegfR expression and not just more Vegf, we measured the amount of VegfR at P17 after OIR in the control and $Fb^{-/-}$ mice and found no difference in expression levels (Fig. 3*C*, *D*).

Although our Vegf data suggest that there is no change in growth stimulation, they are not a direct measurement of endothelial cell proliferation. To directly determine whether there is enhanced neovessel growth in $Fb^{-/-}$ mice, we quantitated the amount of endothelial cell proliferation at P17. After exposure to OIR, the wild-type control and $Fb^{-/-}$ mice were injected intraperitoneally with EdU, a thymidine analogue that intercalates into the DNA of proliferating cells, and the eyes were collected at P17 for sectioning. We found that cell proliferation was restricted to endothelial cells (**Fig. 4*A***) and that there was no change in the amount of endothelial cell proliferation between the wild-type and $Fb^{-/-}$ mice (32.6±1.56 and 32.8±1.76%, respectively; Fig. 4*B*). Together, our data indicate that, in the $Fb^{-/-}$ mice, the increase in neovessels was not a consequence of higher levels of Vegf or neovessel proliferation, but rather may have been the result of decreased

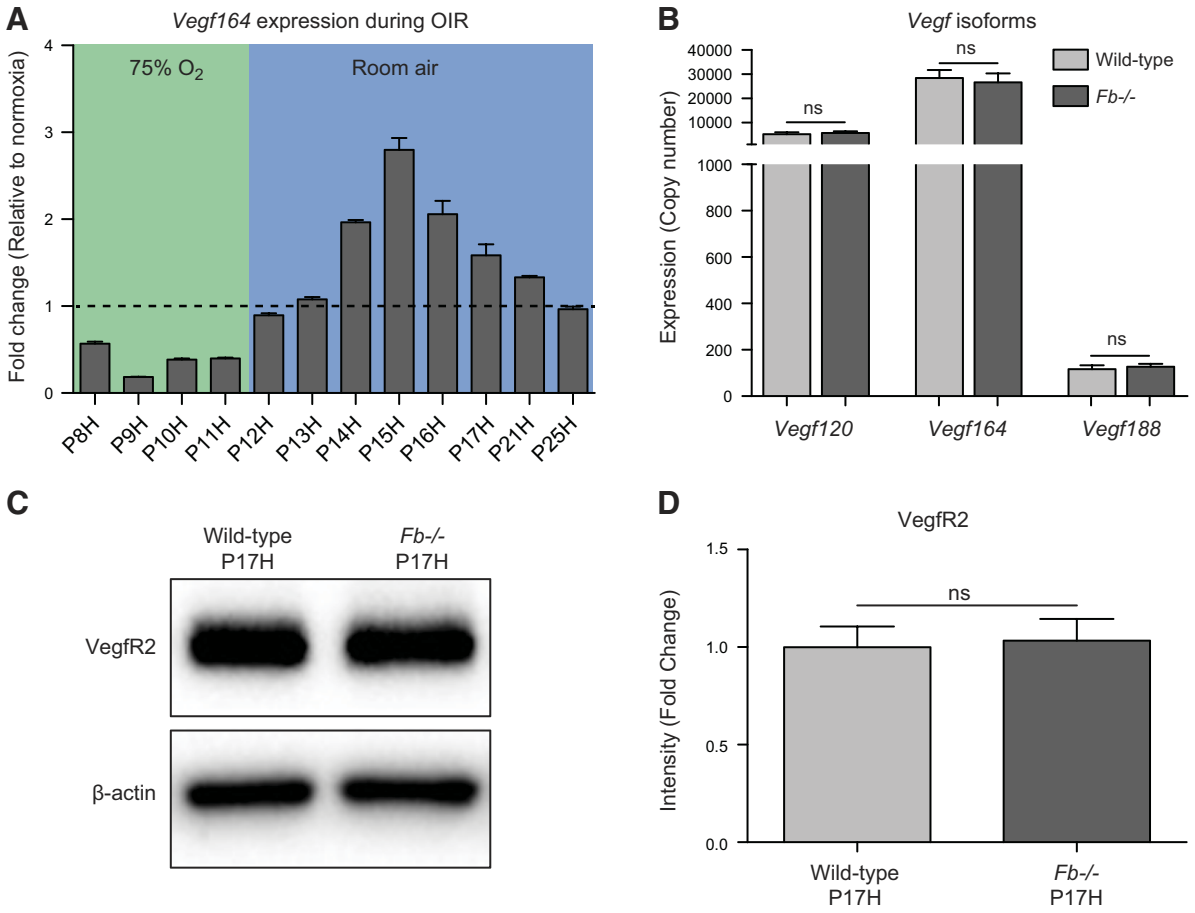

Figure 3. Vegf expression is not altered in $Fb^{-/-}$ mice. *A*) *Vegf164* expression in the retina measured by RT-PCR during the time course of the OIR model (n=6 eyes/time point). Green shading indicates time spent in high oxygen; blue shading, time spent in room air. Dotted black line represents the normoxia control used to normalize each time point. Therefore, anything below the line is a decrease in expression, and anything above the line is an increase. During exposure to high oxygen, *Vegf164* expression was repressed (P8–P12). When the mice were returned to room air, *Vegf164* expression increased (P13–P25). *B*) RT-PCR for gene expression of the *Vegf* isoforms *120*, *164*, and *188* in the retina of P17 hyperoxia wild-type and $Fb^{-/-}$ mice. Each isoform is expressed as the mRNA copy number normalized to an unchanging control gene, to show relative gene expression levels in the retina. There are no significant expression changes for any of the isoforms between wild-type and $Fb^{-/-}$ mice. The most abundantly expressed isoform in the retina is *Vegf164* (n=5 eyes/group). *C*) Representative Western blot of VegfR2 for $Fb^{-/-}$ and wild-type mice at P17 after OIR treatment. Equal concentrations of protein were loaded, with β-actin serving as an internal loading control. *D*) Quantitation of band intensities from 3 independent Western blots for $Fb^{-/-}$ and wild-type mice at P17 after OIR treatment. Band intensities were measured using densitometry and normalized to β-actin (n=6 eyes pooled/group). ns, not significant. Error bars = SEM.

removal of neovessels, leading to an accumulation over time.

The alternative pathway is activated on neovessels

Activation of the alternative complement pathway results in deposition of Fb on targets for immune clearance (13). Fb expression was rapidly induced on return to room air, at both the message (**Fig. 5*A***) and protein (Fig. 5*B*) levels. The increase in Fb expression corresponded to the phase in which neovessels form and likely promoted their disappearance. To determine whether the alternative pathway is activated on neovessels, we stained retinal sections for Fb and found that it was deposited on neovessels at P17 (Fig. 5*C*) and in fact throughout the entire neovascular phase, starting when the neovessels first developed (P14–P17) and through regression (P17–P25) (Supplemental Fig. S2). Fb did not colocalize with vessels in retinas of mice without disease (Supplemental Fig. S3). In addition, it did not colocalize with pathological neovessels in the mice that lacked a functional alternative complement pathway (P17H, $Fb^{-/-}$ mice; Fig. 5*D*). These data suggest that a key component of the alternative complement pathway, Fb, is primarily associated with retinal neovessels and not with normal vasculature.

Alternative pathway activation promotes neovessel apoptosis

To determine whether the increase in neovessels in $Fb^{-/-}$ mice is a result of decreased alternative pathway targeting, we assessed cell death in neovessels at P17 after OIR. To evoke cell death, the complement cas-

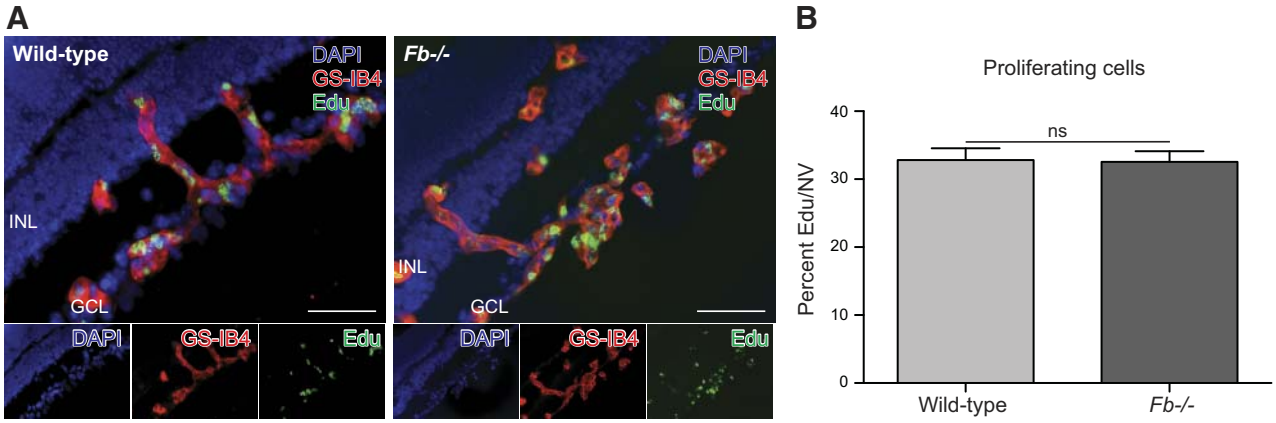

Figure 4. Rate of neovessel proliferation is unchanged in $Fb^{-/-}$ or wild-type mice after OIR. *A*) Representative images of retinal cross sections at P17 after OIR from wild-type mice (left panel) and $Fb^{-/-}$ mice (right panel) injected with the thymidine analogue EdU, to label proliferating cells. Top: representative merged images of EdU (green) colabeled with isolectin B4 (red) and DAPI (blue) in sections from wild-type (left panel) and $Fb^{-/-}$ (right panel) mice. Bottom: individual channels for DAPI (left, blue), GS-IB4 (center, red), and EdU (right, green). GCL, ganglion cell layer. Scale bars = 50 μm. *B*) Quantitation of EdU-positive cells at P17 after OIR in wild-type (32.6±1.56) and $Fb^{-/-}$ (32.8±1.76) mice expressed as the number of EdU-positive cells as a percentage of the neovascular area (wild-type, n=4; $Fb^{-/-}$, n=4). ns, not significant. Error bars = SEM.

cades ultimately form the membrane attack complex (MAC; C5b-9; ref. 14). This complex has been associated with clearance of targeted tissue through apoptosis (32). Given the alternative pathway's targeting of neovessels, we sought to determine whether apoptosis is induced in these cells. We used TUNEL to assess apoptosis in neovessels of wild-type mice after OIR at P17, just before regression in this model. We found that

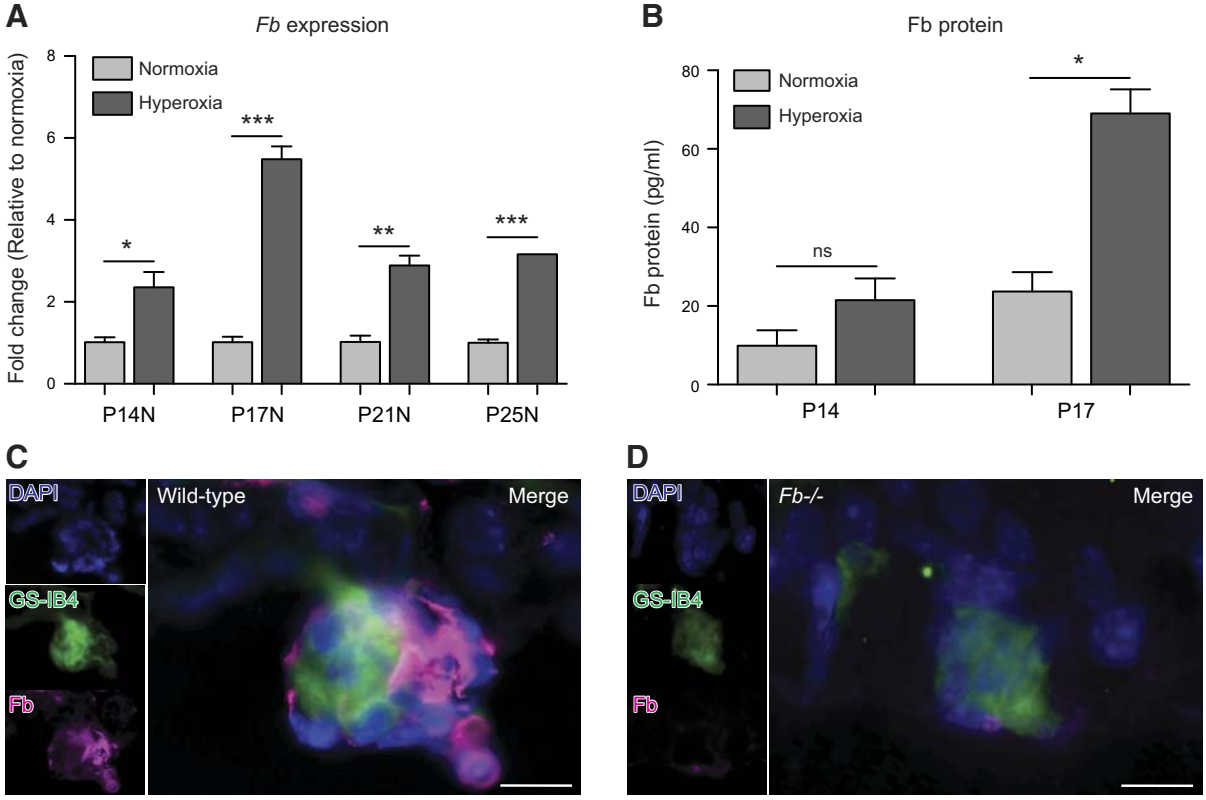

Figure 5. Fb production is increased on neovessels after OIR. *A*) *Fb* retina gene expression in wild-type OIR mice at the indicated time points (n=6 eyes/time point). *Fb* gene expression increased after OIR (hyperoxia), nearly 6-fold at P17, relative to expression in control mice kept in room air (normoxia). *B*) Fb retina protein was significantly elevated at P17 after OIR (hyperoxia) compared to control mice kept in room air (normoxia) (n=6 eyes/time point). *C, D*) Fb colocalized with neovessels after OIR in wild-type mice (*C*), but not in the corresponding $Fb^{-/-}$ control (*D*). Representative images at P17 after OIR colabeled with isolectin B4 (green), Fb (purple), and DAPI (blue) Scale bars = 40 μm. ns, not significant. Error bars = SEM. $*P < 0.05$, $**P < 0.01$, $***P < 0.001$.

apoptosis was restricted to neovessels and did not affect the surrounding mature vessels (Supplemental Fig. S4). We then quantitated the number of endothelial cells undergoing apoptosis in each neovessel and found that the $Fb^{-/-}$ mice had far fewer apoptotic cells than the control (3.49±1.36 and 31.22±4.8% for WT and $Fb^{-/-}$, respectively; **Fig. 6*A*, *B***), indicating that there is an accumulation of neovessels due to the reduction in apoptosis.

The C3 convertase inhibitor Cd55 is down-regulated in neovessels, suggesting a mode of alternative pathway amplification

Finally, we addressed how neovessels might be more susceptible to complement-mediated apoptosis than are the surrounding cells. A characteristic of neovessels is hypoxia (33, 34) and the expression of Cd55 (decay-accelerating factor), a potent negative regulator of the alternative pathway (18), has been shown to be down-regulated in hypoxic conditions (35–39). During alternative pathway activation, the C3 convertase can cleave many molecules of C3 to C3a/C3b, thereby intensifying complement activation (40). Foreign surfaces are generally devoid of membrane regulatory proteins that inhibit the C3 convertase, leading to complement amplification. In contrast, host cells are protected from the harmful effects of complement through cell surface–associated, convertase-regulatory proteins (18, 40). Cd55 acts to avert opsonization and damage to self-cells at the site of complement initiation by inactivating the C3 and C5 convertase enzymes (18, 40). Cd55 hastens the decay of the convertase by releasing Bb (40). Therefore, to test whether hypoxia leads to Cd55 down-regulation in endothelial cells, we subjected HUVECs to low oxygen (1% O_2) and assessed Cd55 expression over time by RT-PCR. We found that, after 24 h, the expression levels of *Cd55* were significantly suppressed (**Fig. 7*A*, *B***). Notably, when the same cells were placed back into atmospheric oxygen for another 24 h, *Cd55* expression levels returned to near normal (Fig. 7*A*).

To determine whether Cd55 is down-regulated in neovessels in the OIR model we used LCM to isolate each retinal layer, as well as the vasculature, and then assessed the expression pattern of *Cd55* in the retina (**Fig. 8*A***). In P17 wild-type mice kept in room air (normoxia), *Cd55* expression was evident in all the layers, but was most prominent in the retinal vasculature (Fig. 8*B*). Since the retinal vasculature of normoxic mice expresses relatively high levels of *Cd55*, we compared their expression to neovessels. Vessels from normoxic retinas and pathological neovessels from OIR retinas were isolated by LCM for analysis by RT-PCR (Fig. 8*C*). Normal vessels expressed relatively high levels of *Cd55* mRNA, whereas Cd55 expression was significantly repressed in pathological neovessels (Fig. 8*D*). Therefore, taken together, these data indicate that the hypoxic environment in which neovessels exist (33, 34) leads to the down-regulation of *Cd55*, resulting in susceptibility to alternative pathway–mediated clearance, whereas the mature vasculature remains protected by higher expression of *Cd55*.

DISCUSSION

Neovascularization is a major cause of blindness (3), making the suppression of dysfunctional neovessels while protecting normal vessels of great therapeutic interest. In most ROP cases, neovessels spontaneously regress while normal vessels persist (10). To date, there has been a gap in our knowledge of how this occurs and

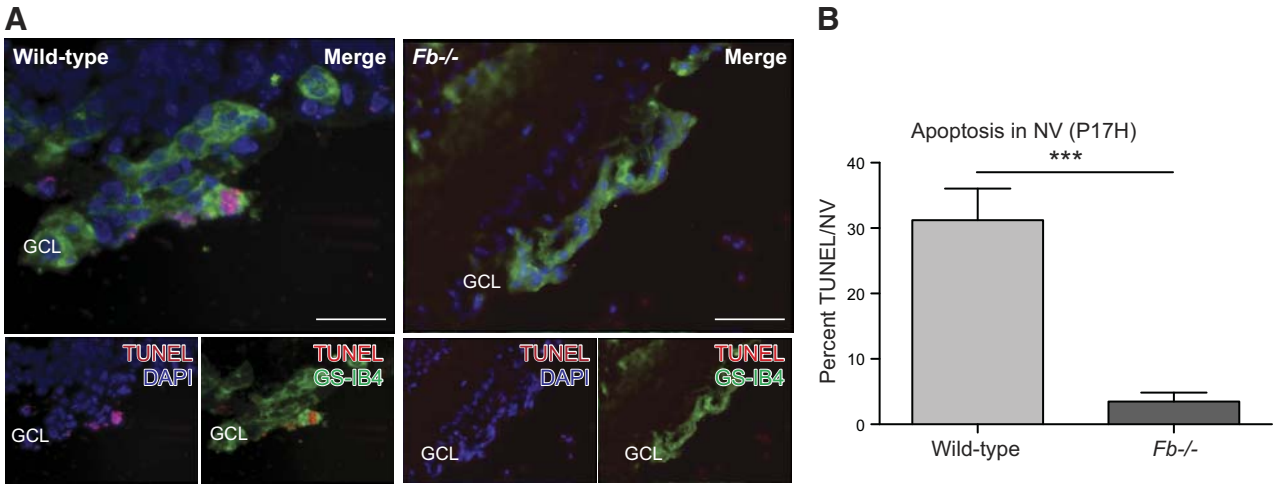

Figure 6. Rate of apoptosis is reduced in $Fb^{-/-}$ mice. *A*) Representative images of retinal cross-sections at P17 after OIR from wild-type mice (left panel) and $Fb^{-/-}$ mice (right panel) colabeled with DAPI (blue), isolectin B4 (green), and TUNEL (red) and then merged (bottom). GCL, ganglion cell layer. Scale bars = 20 μm. Although there was an abundance of TUNEL-positive cells in neovessels of wild-type mice, they were rarely found in $Fb^{-/-}$ mice. *B*) Quantitation of TUNEL-positive cells at P17 after OIR in wild-type and $Fb^{-/-}$ mice expressed as the number of TUNEL-positive cells as a percentage of the neovascular area (wild-type, n=5 eyes; $Fb^{-/-}$, n=6 eyes). Error bars = SEM. ***$P < 0.001$.

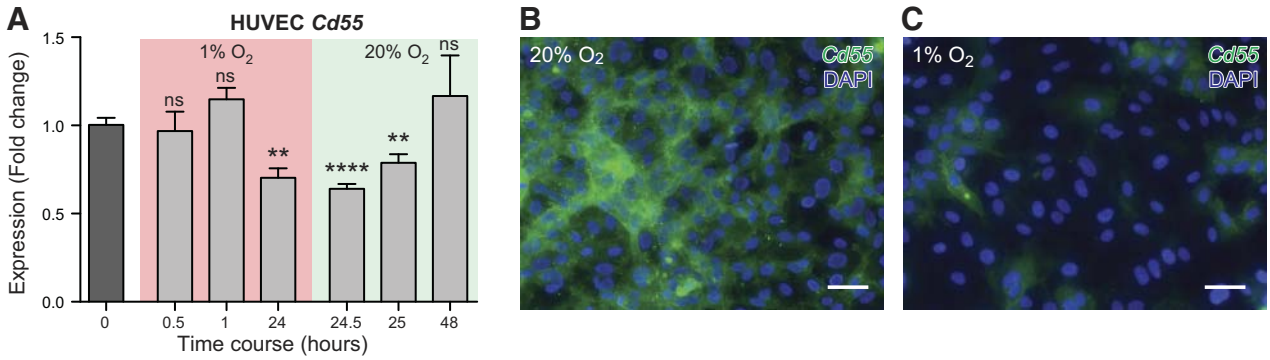

Figure 7. Cd55 is down-regulated in HUVECs cultured in hypoxic conditions. *A*) RT-PCR for *Cd55* expression in HUVECs placed in 1% O_2 (red shading) for 24 h and returned to 20% O_2 (green shading) for another 24 h. After 24 h in 1% O_2, expression levels of *Cd55* were reduced ≈40% and rebounded after a return to 20% O_2. Data are the average of 3 independent experiments. ns, not significant. Error bars = SEM. $^{**}P < 0.01$, $^{****}P < 0.0001$. *B*) Immunohistochemistry for Cd55 (green) colabeled with DAPI (blue) in HUVECs cultured for 24 h in atmospheric O_2. *C*) Immunohistochemistry of Cd55 (green) colabeled with DAPI (blue) in HUVECs cultured in 1% O_2 for 24 h. Scale bars = 50 μm.

specifically how neovessels are distinguished from normal vessels. In this study, we found that the alternative complement pathway is involved in the control of neovessel formation and regression. Numerous diseases have linked complement activation to disease exacerbation, including age-related macular degeneration (41), atypical hemolytic uremic syndrome (42), and paroxysmal nocturnal hemoglobinuria (14, 43). To the contrary, this work describes a new, beneficial function for the alternative complement pathway in retinopathy, involving a form of protective autoimmunity that allows the body to distinguish between pathological neovessels and normal vessels.

A major regulatory function of the alternative pathway is to remain in a primed state for an immediate response to the presence of foreign pathogens or damaged cells (14). Previous work has identified that $C3^{-/-}$ and $C5aR^{-/-}$ mice develop enhanced angiogenesis in an OIR model (12). That study elegantly illustrated the importance of the C5aR for switching macrophages to an M1 antiangiogenic signature, although it only partially explained how $C3^{-/-}$ mice develop enhanced angiogenesis. Our work complements these findings by addressing how the upstream components of the alternative pathway are able to specifically target neovessels for removal. Furthermore, we looked at a time-dependent activation of complement on neovessels by spanning neovessel development and regression, using $Fb^{-/-}$ mice, which lack a rate-limiting protein of the alternative pathway rather than the downstream central C3 protein. By combining the results of the previous study (12) with those of our work, we can begin to formulate a mechanism for how the alternative pathway orchestrates the removal of neovessels. We found that mice deficient in the alternative complement pathway had enhanced neovessel development compared with control mice (Fig. 2 and Supplemental Fig. S1). The difference in neovessel formation did not appear to be a consequence of elevated Vegf release in $Fb^{-/-}$ mice (Fig. 3). In agreement with unchanged levels of Vegf, we found that the growth rate of endothelial cells was unaltered in $Fb^{-/-}$ mice relative to that in the controls (Fig. 4), a result that suggests that the increase in neovessels is not due to enhanced proliferation.

In distinguishing between neovessels and normal vessels, a major regulatory molecule in the alternative pathway, Fb (44, 45), localizes to neovessels in retinas of mice subjected to OIR (Fig. 5 and Supplemental Fig. S2) but does not associate with normal vessels (Supplemental Fig. S3). Complement ultimately induces cellular destruction through formation of the MAC (or C5b-9), inducing apoptosis (46). In agreement with the notion that alternative complement contributes to neovessel resolution, $Fb^{-/-}$ retinas had fewer TUNEL-positive cells associated with pathological neovessels (Fig. 6), compared to the number in the wild-type controls. Furthermore, we found that apoptosis was restricted to cells of the neovessels and did not occur in the surrounding cells (Supplemental Fig. S4). This observation correlates with our finding that Fb was restricted to neovessels (Fig. 5 and Supplemental Fig. S2), suggesting that alternative pathway activation on the neovessels leads to apoptosis. These findings are consistent with the idea that complement helps to control targeted neovessel removal without harming the surrounding architecture of the retina.

Finally, we addressed a mechanism by which it is possible for complement to target only the neovasculature. A characteristic of neovessels is hypoxia (33, 34), and we found that, when endothelial cells are kept in hypoxic conditions, Cd55 is temporarily down-regulated (Fig. 7). Therefore, one explanation for preferential activation of the alternative pathway (Fb deposition) on neovessels is that neovessels lack Cd55, a negative regulator of the alternative pathway. Cd55, a membrane-bound regulator that blocks the C3 convertase formation (18) and is essential for alternative pathway amplification, localized with normal vessels but had much lower expression in neoves-

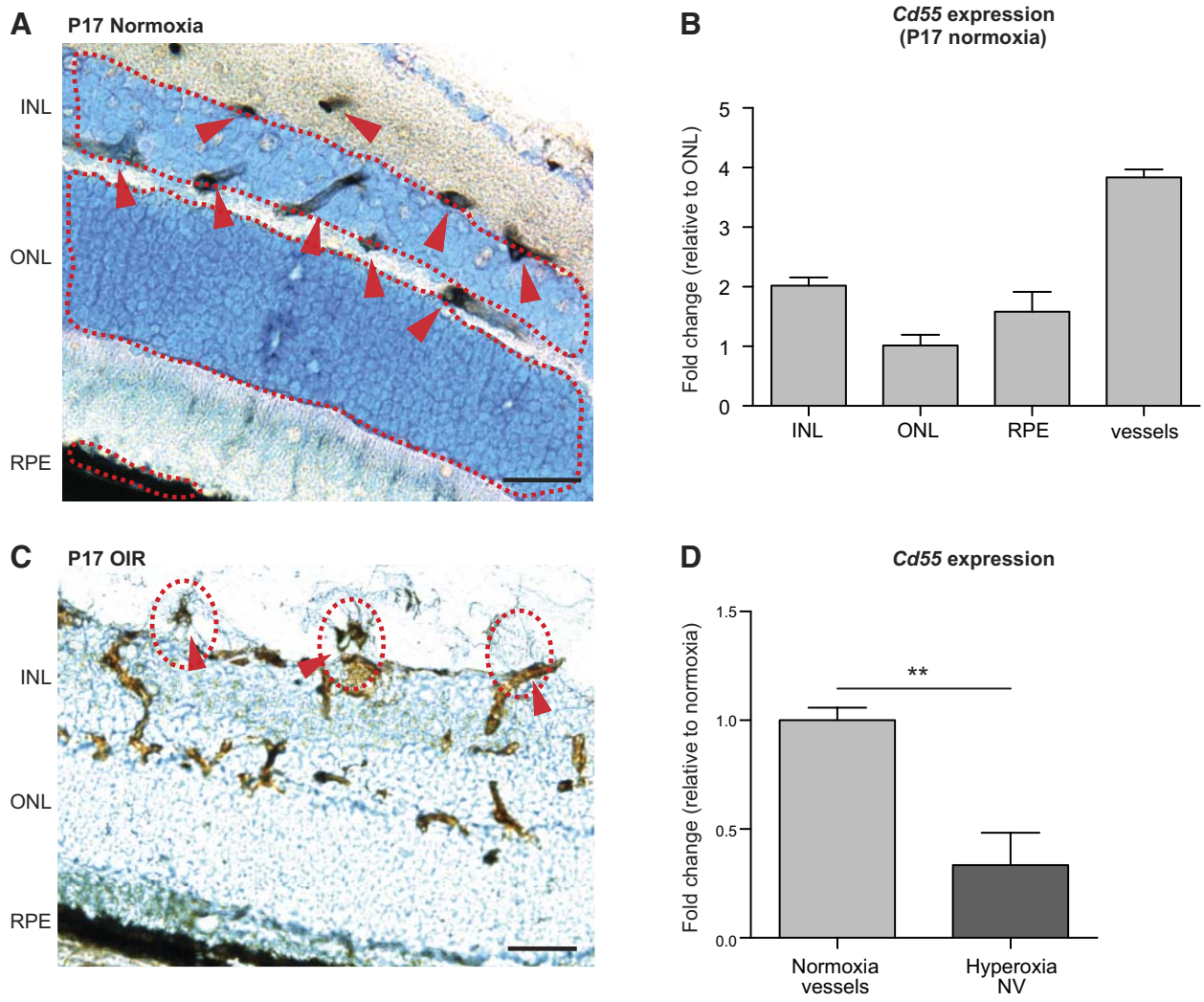

Figure 8. Cd55 is down-regulated in neovessels, suggesting a mode for alternative pathway amplification. *A*) Representative cross-section of a wild-type mouse eye at P17 that was kept in room air (normoxia) and stained with toluidine blue (blue), for identification of cell layers, along with isolectin B4 (brown), to identify mature vessels. Red dotted lines indicate the cell layers, red arrowheads the mature vessels isolated by LCM. Scale bar = 40 μm. *B*) *Cd55* gene expression in the retinal layers and mature vessels from samples isolated by LCM in wild-type P17 mice kept in room air (normoxia; n=3 eyes/cell type). Fold change in expression was standardized to the cell type, with the least amount of *Cd55* gene expression, the ONL. Error bars = SEM. *C*) Representative cross section of an OIR mouse eye at P17 labeled with isolectin B4 (brown) to identify neovessels. Red arrowheads/dotted lines demarcate neovessels isolated by LCM. Scale bar = 40 μm. *D*) Cd55 gene expression in mature vessels of mice kept in room air (normoxia vessels) compared to neovessels (hyperoxia NV) from OIR mice, both at P17 (n=3 eyes/group). $^{**}P < 0.01$.

sels (Fig. 8). Although we found that Cd55 was differentially located on the normal vasculature *vs.* neovessels, it is likely that it is not the only molecule that protects normal vessels, which may be exposed intermittently to high levels of complement (47–49). However, there are data suggesting that Cd55 function is important in normal vessel survival. A recent study identified Cd55 as a key indicator in renal allograft survival. Patients with increased peritubular capillary Cd55 expression had increased graft survival over those with low Cd55 expression (50). Our data are consistent with these findings in patients, thus reinforcing the importance of this regulatory mechanism of complement in controlling the vasculature in disease states.

In summary, these data show differences in components involving the innate immune system between neovessels and normal vessels. We found that the lack of the alternative complement pathway promotes accumulation of neovessels and delays neovessel regression. We postulate that a mechanism of neovessel removal involves the increased susceptibility of pathological neovessels to alternative pathway activation, initiating complement-mediated apoptosis and regression. Although the alternative complement pathway appears to play a role in neovessel regression during retinopathy, it clearly is not the sole regulator of vessel regression, as loss of the alternative pathway does not cause neovessels to persist indefinitely. It is likely that other regulatory

pathways, such as those involving oxygen, are important, as well. FJ

Research reported in this publication was supported by the National Eye Institute of the U.S. National Institutes of Health (NIH) under award numbers R01EY022084-01/S1 (K.M.C.), EY020633-02 and AI068730 (J.D.L.), T32EY007145 (J.H.S.), and P30EY014104. The content is solely the responsibility of the authors and does not necessarily represent the official views of the NIH. Additional support was provided by the Howe Laboratory endowment of the Massachusetts Eye and Ear Infirmary; March of Dimes Foundation (5-FY09-535); a Research to Prevent Blindness unrestricted grant; Massachusetts Lions Eye Research Fund, Inc. (K.M.C.); and an award from the Japan Eye Bank Association (to R.Y.).

REFERENCES

1. Folkman, J. (2007) Angiogenesis: an organizing principle for drug discovery? *Nat. Rev. Drug Discov.* **6,** 273–286
2. Moulton, K. S. (2006) Angiogenesis in atherosclerosis: gathering evidence beyond speculation. *Curr. Opin. Lipidol.* **17,** 548–555
3. Stahl, A., Connor, K. M., Sapieha, P., Chen, J., Dennison, R. J., Krah, N. M., Seaward, M. R., Willett, K. L., Aderman, C. M., Guerin, K. I., Hua, J., Lofqvist, C., Hellstrom, A., and Smith, L. E. (2010) The mouse retina as an angiogenesis model. *Invest. Ophthalmol. Vis. Sci.* **51,** 2813–2826
4. Stem, M. S., and Gardner, T. W. (2013) Neurodegeneration in the pathogenesis of diabetic retinopathy: molecular mechanisms and therapeutic implications. *Curr. Med. Chem.* **20,** 3241–3250
5. Chen, J., and Smith, L. E. (2007) Retinopathy of prematurity. *Angiogenesis* **10,** 133–140
6. Penn, J. S., Madan, A., Caldwell, R. B., Bartoli, M., Caldwell, R. W., and Hartnett, M. E. (2008) Vascular endothelial growth factor in eye disease. *Prog. Retin. Eye Res.* **27,** 331–371
7. Connor, K. M., SanGiovanni, J. P., Lofqvist, C., Aderman, C. M., Chen, J., Higuchi, A., Hong, S., Pravda, E. A., Majchrzak, S., Carper, D., Hellstrom, A., Kang, J. X., Chew, E. Y., Salem, N., Jr., Serhan, C. N., and Smith, L. E. (2007) Increased dietary intake of omega-3-polyunsaturated fatty acids reduces pathological retinal angiogenesis. *Nat. Med.* **13,** 868–873
8. Gardiner, T. A., Gibson, D. S., de Gooyer, T. E., de la Cruz, V. F., McDonald, D. M., and Stitt, A. W. (2005) Inhibition of tumor necrosis factor-alpha improves physiological angiogenesis and reduces pathological neovascularization in ischemic retinopathy. *Am. J. Pathol.* **166,** 637–644
9. Connor, K. M., Krah, N. M., Dennison, R. J., Aderman, C. M., Chen, J., Guerin, K. I., Sapieha, P., Stahl, A., Willett, K. L., and Smith, L. E. (2009) Quantification of oxygen-induced retinopathy in the mouse: a model of vessel loss, vessel regrowth and pathological angiogenesis. *Nat. Protocols* **4,** 1565–1573
10. Mechoulam, H., and Pierce, E. A. (2003) Retinopathy of prematurity: molecular pathology and therapeutic strategies. *Am J. Pharmacogenomics* **3,** 261–277
11. Adamis, A. P., and Berman, A. J. (2008) Immunological mechanisms in the pathogenesis of diabetic retinopathy. *Semin. Immunopathol.* **30,** 65–84
12. Langer, H. F., Chung, K. J., Orlova, V. V., Choi, E. Y., Kaul, S., Kruhlak, M. J., Alatsatianos, M., DeAngelis, R. A., Roche, P. A., Magotti, P., Li, X., Economopoulou, M., Rafail, S., Lambris, J. D., and Chavakis, T. (2010) Complement-mediated inhibition of neovascularization reveals a point of convergence between innate immunity and angiogenesis. *Blood* **116,** 4395–4403
13. Ricklin, D., Hajishengallis, G., Yang, K., and Lambris, J. D. (2010) Complement: a key system for immune surveillance and homeostasis. *Nat. Immunol.* **11,** 785–797
14. Ricklin, D., and Lambris, J. D. (2013) Complement in immune and inflammatory disorders: pathophysiological mechanisms. *J. Immunol.* **190,** 3831–3838
15. Nilsson, B., and Nilsson Ekdahl, K. (2012) The tick-over theory revisited: is C3 a contact-activated protein? *Immunobiology* **217,** 1106–1110
16. Forneris, F., Ricklin, D., Wu, J., Tzekou, A., Wallace, R. S., Lambris, J. D., and Gros, P. (2010) Structures of C3b in complex with factors B and D give insight into complement convertase formation. *Science* **330,** 1816–1820
17. Kemper, C., Leung, M., Stephensen, C. B., Pinkert, C. A., Liszewski, M. K., Cattaneo, R., and Atkinson, J. P. (2001) Membrane cofactor protein (MCP; CD46) expression in transgenic mice. *Clin. Exp. Immunol.* **124,** 180–189
18. Harris, C. L., Rushmere, N. K., and Morgan, B. P. (1999) Molecular and functional analysis of mouse decay accelerating factor (Cd55). *Biochem. J.* **341,** 821–829
19. Hamilton, K. K., Ji, Z., Rollins, S., Stewart, B. H., and Sims, P. J. (1990) Regulatory control of the terminal complement proteins at the surface of human endothelial cells: neutralization of a C5b-9 inhibitor by antibody to CD59. *Blood* **76,** 2572–2577
20. Rollins, S. A., and Sims, P. J. (1990) The complement-inhibitory activity of CD59 resides in its capacity to block incorporation of C9 into membrane C5b-9. *J. Immunol.* **144,** 3478–3483
21. Hourcade, D., Liszewski, M. K., Krych-Goldberg, M., and Atkinson, J. P. (2000) Functional domains, structural variations and pathogen interactions of MCP, DAF and CR1. *Immunopharmacology* **49,** 103–116
22. Zhang, L., Yang, N., Park, J. W., Katsaros, D., Fracchioli, S., Cao, G., O'Brien-Jenkins, A., Randall, T. C., Rubin, S. C., and Coukos, G. (2003) Tumor-derived vascular endothelial growth factor up-regulates angiopoietin-2 in host endothelium and destabilizes host vasculature, supporting angiogenesis in ovarian cancer. *Cancer Res.* **63,** 3403–3412
23. Morita, M., Ohneda, O., Yamashita, T., Takahashi, S., Suzuki, N., Nakajima, O., Kawauchi, S., Ema, M., Shibahara, S., Udono, T., Tomita, K., Tamai, M., Sogawa, K., Yamamoto, M., and Fujii-Kuriyama, Y. (2003) HLF/HIF-2alpha is a key factor in retinopathy of prematurity in association with erythropoietin. *EMBO J.* **22,** 1134–1146
24. Weidemann, A., Krohne, T. U., Aguilar, E., Kurihara, T., Takeda, N., Dorrell, M. I., Simon, M. C., Haase, V. H., Friedlander, M., and Johnson, R. S. (2010) Astrocyte hypoxic response is essential for pathological but not developmental angiogenesis of the retina. *Glia* **58,** 1177–1185
25. Sasidharan, C. K., Kumar, M. S., Anoop, P., Syamala, B., and Das, B. N. (2003) Spontaneous regression of retinopathy of prematurity. *Indian J. Pediatr.* **70,** 359–360
26. Pierce, E. A., Avery, R. L., Foley, E. D., Aiello, L. P., and Smith, L. E. (1995) Vascular endothelial growth factor/vascular permeability factor expression in a mouse model of retinal neovascularization. *Proc. Natl. Acad. Sci. U.S.A.* **92,** 905–909
27. Aiello, L. P., Pierce, E. A., Foley, E. D., Takagi, H., Chen, H., Riddle, L., Ferrara, N., King, G. L., and Smith, L. E. (1995) Suppression of retinal neovascularization in vivo by inhibition of vascular endothelial growth factor (VEGF) using soluble VEGF-receptor chimeric proteins. *Proc. Natl. Acad. Sci. U.S.A.* **92,** 10457–10461
28. Ozaki, H., Seo, M. S., Ozaki, K., Yamada, H., Yamada, E., Okamoto, N., Hofmann, F., Wood, J. M., and Campochiaro, P. A. (2000) Blockade of vascular endothelial cell growth factor receptor signaling is sufficient to completely prevent retinal neovascularization. *Am. J. Pathol.* **156,** 697–707
29. Saishin, Y., Takahashi, K., Lima e Silva, R., Hylton, D., Rudge, J. S., Wiegand, S. J., and Campochiaro, P. A. (2003) VEGF-TRAP(R1R2) suppresses choroidal neovascularization and VEGF-induced breakdown of the blood-retinal barrier. *J. Cell. Physiol.* **195,** 241–248
30. Seo, M. S., Kwak, N., Ozaki, H., Yamada, H., Okamoto, N., Yamada, E., Fabbro, D., Hofmann, F., Wood, J. M., and Campochiaro, P. A. (1999) Dramatic inhibition of retinal and choroidal neovascularization by oral administration of a kinase inhibitor. *Am. J. Pathol.* **154,** 1743–1753
31. Pierce, E. A., Foley, E. D., and Smith, L. E. (1996) Regulation of vascular endothelial growth factor by oxygen in a model of retinopathy of prematurity. *Arch. Ophthalmol.* **114,** 1219–1228
32. Rus, H., Cudrici, C., David, S., and Niculescu, F. (2006) The complement system in central nervous system diseases. *Autoimmunity* **39,** 395–402

33. Hoang, M. V., Smith, L. E., and Senger, D. R. (2011) Calpain inhibitors reduce retinal hypoxia in ischemic retinopathy by improving neovascular architecture and functional perfusion. *Biochim. Biophys. Acta* **1812,** 549–557
34. Hoang, M. V., Smith, L. E., and Senger, D. R. (2010) Moderate GSK-3beta inhibition improves neovascular architecture, reduces vascular leakage, and reduces retinal hypoxia in a model of ischemic retinopathy. *Angiogenesis* **13,** 269–277
35. Okroj, M., Corrales, L., Stokowska, A., Pio, R., and Blom, A. M. (2009) Hypoxia increases susceptibility of non-small cell lung cancer cells to complement attack. *Cancer Immunol. Immunother.* **58,** 1771–1780
36. Pedersen, E. D., Froyland, E., Kvissel, A. K., Pharo, A. M., Skalhegg, B. S., Rootwelt, T., and Mollnes, T. E. (2007) Expression of complement regulators and receptors on human NT2-N neurons–effect of hypoxia and reoxygenation. *Mol. Immunol.* **44,** 2459–2468
37. Suzuki, H., Lasbury, M. E., Fan, L., Vittal, R., Mickler, E. A., Benson, H. L., Shilling, R., Wu, Q., Weber, D. J., Wagner, S. R., Lasaro, M., Devore, D., Wang, Y., Sandusky, G. E., Lipking, K., Pandya, P., Reynolds, J., Love, R., Wozniak, T., Gu, H., Brown, K. M., and Wilkes, D. S. (2013) Role of complement activation in obliterative bronchiolitis post-lung transplantation. *J. Immunol.* **191,** 4431–4439
38. Zimmermann, A., Gerber, H., Nussenzweig, V., and Isliker, H. (1990) Decay-accelerating factor in the cardiomyocytes of normal individuals and patients with myocardial infarction. *Virch. Arch. A Pathol. Anat. Histopathol.* **417,** 299–304
39. Vakeva, A., and Meri, S. (1998) Complement activation and regulator expression after anoxic injury of human endothelial cells. *APMIS* **106,** 1149–1156
40. Harris, C. L., Pettigrew, D. M., Lea, S. M., and Morgan, B. P. (2007) Decay-accelerating factor must bind both components of the complement alternative pathway C3 convertase to mediate efficient decay. *J. Immunol.* **178,** 352–359
41. Yanai, R., Thanos, A., and Connor, K. M. (2012) Complement involvement in neovascular ocular diseases. *Adv. Exp. Med Biol.* **946,** 161–183
42. Roumenina, L. T., Loirat, C., Dragon-Durey, M. A., Halbwachs-Mecarelli, L., Sautes-Fridman, C., and Fremeaux-Bacchi, V. (2011) Alternative complement pathway assessment in patients with atypical HUS. *J. Immunol. Methods* **365,** 8–26
43. Van der Schoot, C. E., Huizinga, T. W., van 't Veer-Korthof, E. T., Wijmans, R., Pinkster, J., and von dem Borne, A. E. (1990) Deficiency of glycosyl-phosphatidylinositol-linked membrane glycoproteins of leukocytes in paroxysmal nocturnal hemoglobinuria, description of a new diagnostic cytofluorometric assay. *Blood* **76,** 1853–1859
44. Walport, M. J. (2001) Complement: first of two parts. *N. Engl. J. Med.* **344,** 1058–1066
45. Walport, M. J. (2001) Complement: second of two parts. *N. Engl. J. Med.* **344,** 1140–1144
46. Nauta, A. J., Daha, M. R., Tijsma, O., van de Water, B., Tedesco, F., and Roos, A. (2002) The membrane attack complex of complement induces caspase activation and apoptosis. *Eur. J. Immunol.* **32,** 783–792
47. Kim, D. D., and Song, W. C. (2006) Membrane complement regulatory proteins. *Clin. Immunol.* **118,** 127–136
48. Ramaglia, V., King, R. H., Morgan, B. P., and Baas, F. (2009) Deficiency of the complement regulator CD59a exacerbates Wallerian degeneration. *Mol. Immunol.* **46,** 1892–1896
49. Song, W. C. (2004) Membrane complement regulatory proteins in autoimmune and inflammatory tissue injury. *Curr. Dir. Autoimmun.* **7,** 181–199
50. Brodsky, S. V., Nadasdy, G. M., Pelletier, R., Satoskar, A., Birmingham, D. J., Hadley, G. A., Obeidat, K., and Nadasdy, T. (2009) Expression of the decay-accelerating factor (Cd55) in renal transplants: a possible prediction marker of allograft survival. *Transplantation* **88,** 457–464

Received for publication February 5, 2014.
Accepted for publication March 17, 2014.